# Twinning-, Polytypism-, and Polarity-Induced Morphological Modulation in Nonplanar Nanostructures with van der Waals Epitaxy

*Muhammad Iqbal Bakti Utama, Maria de la Mata, Cesar Magen, Jordi Arbiol,* and Qihua Xiong**

**Twinning, polytypism, and polarity are important aspects in nanostructural growth since their presence can affect various properties of the as-grown products. The morphology of nanostructures grown via van der Waals epitaxy is shown to be strongly influenced by the twinning density and the presence of polytypism within the nanostructures, while the growth direction is driven by the compound polarity. With ZnTe as the model material, vertically aligned nanorods are successfully produced with variable cross-section and branched crystals (tripods and tetrapods) on only a single type of substrate. Van der Waals epitaxy contributes by relaxing the lattice-mismatch requirements for epitaxial growth and by enabling a variety of crystal planes in the initial stages of the growth to be interfaced to the substrate, regardless of the polarity of the epitaxial material. These results may provide more flexibility in tuning rationally the morphology of epitaxial nanostructures into other shapes with higher complexity by routine adjustment of growth environment.**

## 1. Introduction

Controlling the crystalline quality and defects in a nanostructured material are of primary issues to accomplish within a synthesis procedure. Due to the minute size of nanostructures, even minor alterations of the crystalline properties might have significant effects on the ensuing material and physical characteristics of the nanostructures. Nanowires from II-VI semiconductors—as an important example of nanostructures due to their excellent prospective applications in many technological fields[1]—are particularly prone to defects during the crystal growth. Crystalline imperfection, especially twinning and polytypism,[2] are often produced during the synthesis process as a means of energy minimization and stabilization of high energy surfaces.[3] Reason being, the compounds comprising the II–VI groups could have multiple crystalline phases that are close in energy, i.e., the hexagonal wurtzite (WZ) and the cubic zincblende (ZB) phases. Nevertheless, the presence of twinning and polytypism are not always deleterious. Those planar defects are exploitable in realizing interesting concepts, such as the construction of multiquantum well superlattice due to the difference in electronic band structure of WZ and ZB phases[4] and the growth of branched nanocrystals (e.g., tetrapods[5] and tripods[6]) with high structural complexity.

The progress of research in the phenomenology and theoretical aspects of twinning and polytypism in nanostructures, particularly nanowire arrays, are encouraging. However, the

M. I. B. Utama, Prof. Q. H. Xiong
Division of Physics and Applied Physics
School of Physical and Mathematical Sciences
Nanyang Technological University
637371, Singapore
E-mail: Qihua@ntu.edu.sg
M. de la Mata, Prof. J. Arbiol
Institut de Ciència de Materials de Barcelona
ICMAB-CSIC, Campus de la UAB, 08193 Bellaterra, Catalonia, Spain
E-mail: arbiol@icrea.cat
Dr. C. Magen
Laboratorio de Microscopías Avanzadas (LMA)
Instituto de Nanociencia de Aragon (INA)–ARAID
Departamento de Fisica de la Materia Condensada
Universidad de Zaragoza
50018 Zaragoza, Spain
Prof. J. Arbiol
Institució Catalana de Recerca i Estudis
Avançats (ICREA)
08010 Barcelona, Catalonia, Spain
Prof. Q. H. Xiong
Division of Microelectronics
School of Electrical and Electronics Engineering
Nanyang Technological University
639798, Singapore

DOI: 10.1002/adfm.201202027

studies on nanowire arrays are conducted mostly on structures that are grown via conventional epitaxy. Such systems are rather limiting since the orientation of the wires is always dictated by the substrate. Besides, the atomic polarity of the wires is also confined to that of the substrate since inversion of polarity across the heterointerface is rarely observed.[7] Moreover, the conventional heteroepitaxial system necessitates that the nanowire material has a lattice matching with the substrate, thus limiting the number of materials that can be prepared into epitaxial form.[8]

In this work, we consider the effect of twinning and polytypism on II–VI nanostructures grown via "van der Waals epitaxy". Van der Waals epitaxy is a mechanism where the overlayers are grown onto substrates whose surface are inert due to the absence of high density of dangling bonds.[9] Unlike that in conventional heteroepitaxy, the heterointerface of substrate-overlayer is not primarily connected via covalent chemical bonds but rather via van der Waals interaction. Several advantages could be acquired from the weaker binding of heterointerface, such as the alleviation of lattice matching conditions for well-crystallized epitaxial growth[10] and hence the possibility to epitaxially grow various range of compounds within a substrate.[6] Van der Waals epitaxy was originally developed for planar thin film structure in 1990s, and the concept is only recently being revisited and attributed for nanostructured materials.[6,11] Thus, many features of the nanostructures grown via van der Waals epitaxy are not yet well-documented. For instance, how twinning and polytypism could affect the growth of crystals in van der Waals epitaxy is still unknown.

We focus the discussion with zinc telluride (ZnTe) as the model compound. By adjusting the growth environment to induce twinning and polytypism in ZnTe crystals, we shall demonstrate that the morphology of the van der Waals epitaxial ZnTe nanostructures could be modulated. Muscovite mica, despite not prevalently used as the substrate for nanostructures,[12] is intentionally chosen as the substrate to comply with the requirement of van der Waals epitaxy.[10,13] We present the vapor-based synthesis approach of (i) vertically aligned nanowire arrays—or also commonly called "nanorods", (ii) epitaxial nanotripods, and (iii) epitaxial nanotetrapods. The morphogenesis of the different morphologies due to twinning and polytypism is corroborated with extensive electron microscopy characterization.

This work is also intended to serve a multitude of purposes. Firstly, the choice of ZnTe as the model compound is motivated by the rarity of studies on the compound in epitaxial nanostructural form as compared to other binary semiconductors. ZnTe has various interesting material properties: it is a natural p-type II-VI semiconductor[14] with a direct bandgap of 2.26 eV at room temperature and is thus an excellent material for photonic devices in the pure green region.[15] ZnTe in nanostructural form also has various potential applications including optoelectronics[16] and thermoelectric devices.[17] Recently, there have been many reports of randomly oriented ZnTe nanowires that do feature twinning.[18] However, the various aspects and implications of twinning and polytypism in ZnTe are not as well understood as III–V materials. Secondly, the ability to grow ZnTe in epitaxial form also served as a demonstration of the effectiveness of van der Waals epitaxy in synthesizing uncommon epitaxial compounds. Thirdly, we show for the first time the synthesis of tetrapod crystals in epitaxial form (until now, only tetrapods in freestanding or colloidal form have been reported).[5] Lastly, this report also shows for the first time a direct polarity visualization in branched crystals that verifies the long-standing hypothesis on the growth mechanism of tripods and tetrapods.

## 2. ZnTe Nanorod Array: Twinning-Induced Morphological Transition

### 2.1. Synthesis Products

For synthesis performed at high temperature, we typically observed the growth of ZnTe nanorods (**Figure 1**). The nanorods have a strong vertical alignment with respect to the

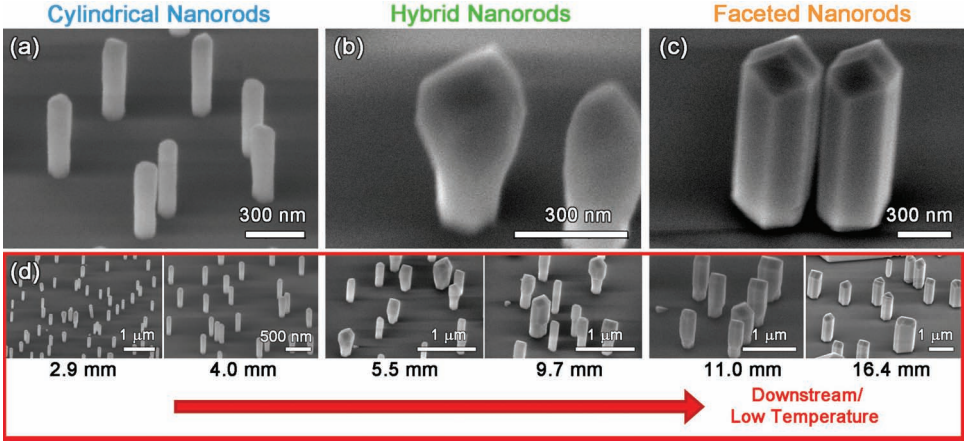


**Figure 1.** SEM images of vertically aligned ZnTe nanorods on muscovite mica in 45° tilted view. a) Nanorods with cylindrical cross-section. b) Hybrid nanorods, possessing a faceted tip and a cylindrical base. c) Completely faceted nanorods. d) Gradual transition of the nanorods morphology with respect to the site of observation, and thus the local temperature of the substrate. The number below the images refers to the distance of the observed site from the upstream edge of the substrate, which has the highest local temperature.

substrate. The nanorods are grown without a buffer layer or any intermediate structures at their base despite the ensuing lattice mismatch between ZnTe and muscovite, in compliance to the typical features of van der Waals epitaxy.[10] The strong vertical alignment of the nanorods without any significant presence of tilted nanorods is a strong benefit offered by the van der Waals epitaxy on muscovite. In contrast, previous works on ZnTe nanorods via conventional heteroepitaxy that necessitates the use of a lattice-matched substrate, e.g., GaAs(100),[19] invariably produce a mixture of vertical and tilted nanorods concurrently within the same substrate.

In our previous article on ZnO nanowire arrays on muscovite,[10] we showed that the van der Waals epitaxy is of incommensurate type. Thus, any parameters regarding the crystallinity of the nanowire material, including their phase and lattice parameters, are irrelevant for the van der Waals epitaxy to occur. Van der Waals epitaxy is also expected not to involve chemical bonding between the epitaxial material and the substrate,[9] also making the chemistry of the epitaxial material an irrelevant issue. Hence, the conclusions regarding the characteristics of the van der Waals epitaxy should also be applicable for the case of the ZnTe nanorod system as described herein.

Interestingly, we observed a variation of nanorod morphology according to the central temperature of the furnace during growth. At the high end of the temperature range, we obtained the growth of nanorods with cylindrical cross-sections (Figure 1a). Meanwhile, at the low end of the growth temperature range where nanorods can still be found, the nanorods are observed to be faceted with hexagonal cross-sections (Figure 1c). In-plane alignment is present between facets of neighboring faceted nanorods, which is as expected for epitaxial growth.[10] To verify the temperature dependence of morphology, we used a longer strip of the substrate during the synthesis. The furnace used in our vapor transport synthesis system has a gradual temperature drop from the center of the furnace (which is the position of the powder source) to both ends of the furnace. Consequently, a long substrate—positioned inside a quartz tube heated on the furnace—should also have a variation of local temperature; the temperature is higher close to the center of the furnace (upstream) and lower further away, in the direction of the carrier gas flow (downstream direction). As a result, we confirmed the presence of cylindrical nanorods at the upstream end and faceted nanorods at the downstream end within a single strip of the substrate (Figure 1d). We also observed the transition of the morphology of nanorods from cylindrical into faceted as we surveyed the substrate from the upstream to downstream sites, exhibiting a hybrid nanorod morphology with a faceted tip and a cylindrical base (Figure 1b).

### 2.2. Characterization of Hybrid Nanorods

To identify the underlying differences between different morphologies of ZnTe nanorods and to determine the mechanism to cause such changes, we performed characterizations with electron microscopy-related techniques on a hybrid ZnTe nanorod (**Figure 2**). Characterization of a hybrid nanorod is expected to provide a meaningful comparison since the presence of faceted and cylindrical segments within a nanorod would isolate only the correlation between the morphology and intrinsic material/physical features (e.g., crystallinity and chemistry) between the cylindrical and faceted nanorod morphologies.

A TEM image of a hybrid ZnTe nanorod is shown in Figure 2a. The coexistence of faceted and cylindrical segments within the nanorod were confirmed with a surface plot (Supporting Information Figure S1): the upper segment of the nanorod is hexagonally faceted while the lower segment is cylindrical. Beside the change in cross-sectional shape, changes in diameter are also noticeable. Energy dispersive X-ray spectroscopy (EDX) scans along the axis of a hybrid nanorod (Supporting Information Figure S2) showed that the composition throughout the nanorod is conserved in a stoichiometric Zn:Te = 1:1 ratio. EDX does have detection sensitivity to only within 1% of the composition, but the EDX characterization is still meaningful in precluding incorporation of major impurity and obvious changes in the final composition of the nanorod product from the possible causes of the morphological transition within the nanorod. We then performed in-depth characterization of the hybrid nanorods with selected area electron diffraction (SAED, Figure 2b–d) and high resolution electron microscopy (HRTEM Figure 2e–g), both of which to probe the crystalline properties, and high angle annular dark field electron microscopy (HAADF-STEM, Figure 2h–j) to characterize the polarity of the nanorod. This characterization focused on three distinct segments of the nanorod, with differently-colored squares in Figure 2a: the faceted upper segment, the middle segment, which is the transition between the faceted cross-section and cylindrical cross-section, and the cylindrical lower segment.

The SAED patterns exhibited by the faceted, the transitional, and the cylindrical segments are distinguishable from each other. For the faceted upper segment, the pattern consists of well-separated spots (Figure 2b). We assign the pattern into two sets of well-defined ZB phase of ZnTe in $[1\bar{1}0]_{ZB}$ and $[\bar{1}10]_{ZB}$ zone axes, both of which indicates that the growth direction of the nanorod is along $[\bar{1}\bar{1}\bar{1}]_{ZB}$ direction, as will be verified later in the polarity study (Figure 2h–j). The simultaneous presence of the patterns from the two zone axes, related by 180° rotation,[20] indicates that the faceted segment contains twin boundaries. However, as only two sets of ZB patterns are noted, the periodicity of twins should be sufficiently low to allow the stacking of complete ZB segments. Meanwhile, the transitional segment exhibits pattern with additional spots and aligned stripes (Figure 2c). In addition to the two zone axes present in the faceted segment, we could also identify set of spots originated from WZ phase ZnTe in $[11\bar{2}0]_{WZ}$, suggesting the occurrence of polytypism.[20–21] Other aligned reflections with different frequencies were also observed and ascribed to the multiplicity of twin periodicity. In other words, the twinning density in the transitional segment is supposedly higher than that in the faceted segment. Even more prominent, the SAED pattern from the base showed a clear aligned line of spots (Figure 2d). The aligned line is suggestive of a high Bragg reflection spot multiplicity induced by nonperiodic twin boundaries. The periodicity of twinning at the cylindrical base must be much higher than that at the faceted and transitional segment, thus inducing a clear change in the atomic plane stacking and creating ZnTe

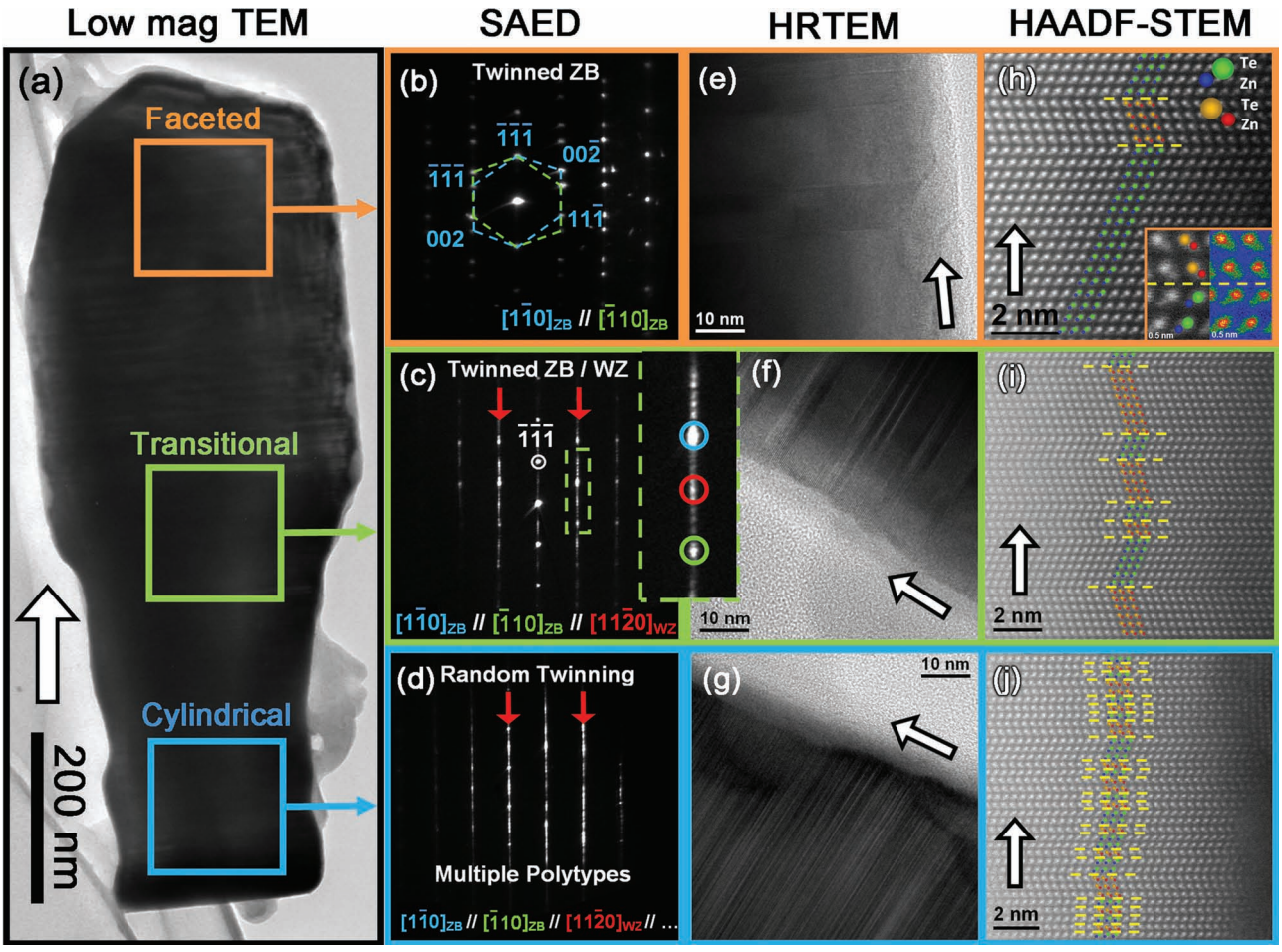


**Figure 2.** Comprehensive electron microscopy characterization of the crystallinity of hybrid nanorods. a) Low magnification TEM image of a hybrid nanorod. Subsequent characterization was focused on different segments of the nanorod as indicated by the colored squares. Top row (orange squares): faceted upper segment. Middle row (green squares): transitional segment. Bottom row (blue squares): cylindrical lower segment. b–d) SAED patterns, showing that the nanorod grew along $<111>_{ZB}$ with features of twinned crystal. Red arrows indicate the streak of twin boundary multiplicity. (Inset in c): zoomed-in image of the region in (c) marked with a green-dashed rectangle. e–g) HRTEM images, showing that the twinning density between the three regions of the nanorod is different. h–j) HAADF-STEM images. The position of atoms within the dumbbells could be distinguished and is marked with spheres as shown in (h), where the dumbbells with different orientation are colored differently. Dashed yellow lines mark the locations of twin boundaries. (Inset in h): RGB temperature false color applied to dumbbells sandwiching a twin boundary. The polarity of the ZnTe is conserved throughout the three regions and across the twin boundaries. White arrows in all panels refer to the growth direction of the nanorod.

polytypic segments. The experimental SAED patterns in the three segments were also corroborated with simulated diffraction patterns (Supporting Information Figure S3), where the interpretation on twinning and polytypism is in agreement with experimental observations.

HRTEM observations validate the presence of twinning in all segments. In agreement to the inference from SAED data, we observe that the twinning density and frequency are different within the three segments: low density at the faceted segment, medium density at the transitional segment, and high density at the cylindrical segment. At the faceted tip (Figure 2e), the typical length between twin boundaries is around 10 nm and wider twin-free segments with widths reaching above 30 nm were found. The twin-free ZB regions are wide enough to allow the completion of ZB stacking, which explains why the SAED provide only two sets of ZB patterns. In contrast, we observed higher density of twin boundaries in the transitional segment (Figure 2f) and even higher density in the cylindrical segment at the base (Figure 2g). The twinning occurred without any apparent periodicity, suggesting that the growth involved a random twinning event. The high density and randomly-distributed twin boundaries in the long range break the atomic ordering into short segments of around a few nanometers. However, the twin boundaries may occur periodically in those short segments, resulting in the formation of various polytpes throughout the nanorod[22] (Supporting Information, Section A), consistent with the conclusion from SAED patterns in Figure 2d. Nevertheless, each atomic layer along the growth direction in every segment is in perfect crystallinity over the whole cross-section of the nanorod as the twin planes dissect the crystal completely; the twin planes are exactly parallel to the growth planes and are perpendicular to the growth direction. Thus, we conclude that the nanorod should grow in a layer-by-layer fashion with a mononucleation center.[21] Meanwhile,

no evidence of axial dislocations were present in our samples, suggesting that the nanorods were unlikely to grow via a screw dislocation mechanism.[23]

The polarity of the nanorod is determined by visualizing ZnTe atomic dumbbells with aberration-corrected HAADF-STEM imaging (Figure 2h–j). Both constituent elements can be resolved and distinguished as Te has a much higher atomic number than Zn ($Z_{Te}$ = 52, $Z_{Zn}$ = 30). In the HAADF observation, Te atoms appear brighter since the *Z*-contrast imaging allows the intensity observed in the image to be in nearly $Z^2$ proportion.[7] The dumbbells are oriented with the Te atoms facing the tip consistently in all segments, implying that the bottom surface of the nanorod contacting the mica substrate is of the polar $(111)_{ZB}$ with Zn-terminated surface. The Te-directed dumbbell orientations justified the assignment of the growth along the $[\bar{1}\bar{1}\bar{1}]_{ZB}$ direction—also commonly referred to as [111]B—as was implicitly assumed in the indexing of SAED patterns. From the image, the variation of twinning density between the different segments is also visible. The polarity of the dumbbells is conserved across the twin boundaries. Therefore, the twin existing in the nanorods is of orthotwin type instead of paratwin, where an inversion of polarity is expected. In orthotwin, the effect of twinning onto the crystal are manifested by the two possible orientations for the dumbbells that are related by a 180° rotation of the structure.[24] The two dumbbell orientations are denoted with illustrations in different colorings (Te in green and Zn in blue for one of the orientations and Te in gold and Zn in red for the other) superimposed onto the image.

### 2.3. The Relevance of the Difference in Twinning Density on the Morphological Transformation in Nanorods

From the characterization of the hybrid ZnTe nanorods, we have established that the morphological difference between the faceted and the cylindrical nanorods is correlated with the difference in twinning density between the two type of nanorods; faceted nanorods contain low density of twinning with wide defect-free ZB segments, whereas cylindrical nanorods are randomly twinned with numerous polytypism. We have also excluded the effect of polarity and compositional variation from the possible causes of the morphological transition observed in Figure 1d, since the two material aspects are conserved throughout the length of a hybrid nanorod. In this section, we discuss the correlation between twinning density and morphological transformation in nanorods. Meanwhile, in-depth investigations on the physical principles and mechanism of twin formation in nanorods/nanowires can be found in various previous reports, some of which will be referred to herein. There are several reports discussing the formation of microfaceting in semiconductor nanowires due to twin boundaries.[24,25] Microfaceting in these structures refers to the change in sidewall faceting orientation due to periodic twinning in the nanowires. In the <111> growth-directed ZB nanowires, each of the twin-free segments of the nanowires has a truncated octahedron morphology consisting of eight {111} planes, with six of them composing the sidewall. Thus, the presence of twin boundaries in the nanowire creates alternating series of octahedral segments, leading to zigzagged edges in the wire.[25b] The nucleation of twinning and the formation of microfaceting was reported to be energetically more favorable than the formation of {112} sidewall facets—which are perpendicular to the growth planes—due to the relatively high surface energy of {112} facets.[26] Presence of twinning allows the two {111} microfacets to replace the {112} sidewall while preserving the growth direction of the nanowires along the atomic stacking direction.

Cutting thin segments along the growth direction from the octahedron will lead to a triangular layer segment with truncated vertices in varying extents that result in variety of shapes, including regular triangle and regular hexagon.[18d,24] If the ZnTe nanorods were to have such microfaceting, the cylindrical nanowires that contain high density of twin boundaries will allow lateral faceting in a very narrow segment between two consecutive twin boundaries. As this change in the microfaceting direction occurs every few atomic planes, the randomly-twinned cylindrical nanorods shall be constructed from the stacking of triangular-like segments of random truncation length. Twinning also rotates the microfaceted segments randomly by 180°. Ultimately, the random contribution of each microfacet will cause the cross-section of the randomly twinned cylindrical nanorods to appear as quasi-circular (Figure 1a).

Of all growth factors that may contribute to the morphological transformation of nanorods, the local temperature on the substrate seemed to be the most dominant, as inferred in the synthesis product shown in Figure 1d. A study on bulk single crystal showed that twinning is a thermodynamically activated event,[27] meaning that a supply of energy is necessary to induce the misplacement in twin stacking in the layer-by-layer growth fashion of nanorods. High local temperature served to satisfy the energy requirement for twinning to occur, which then potentially explains our observation on the growth of highly twinned cylindrical nanorods in the high temperature region and the growth of sparsely twinned faceted nanorods in the low temperature region. The observation where higher temperature growth results into higher density of twinning has also been reported frequently in the growth of nanowires.[24,28]

Other than temperature, we recognize that there are other factors that may have contributed to the formation of twinning and stacking fault density in the structure, which we shall discuss shortly. There are other reported methodologies that exploit different factors and growth parameters (e.g., pressure, precursor molar fraction, and impurities[28]) in controlling the twin density, and we believe that it is conceptually possible to use each of those factors to control the twin density and arrive at the same morphological modulation as reported herein. However, we believe that those factors are not the most relevant in determining the variability of morphology in our synthesis system. Moreover, we argue that the presence of hybrid nanorods with variation of stacking fault and twinning density along the length of the nanorods should not be interpreted as due to variation of growth parameters (including due to flux of vapor species) along with growth time: all nanorods consistently have cylindrical morphology (Figure 1a; high twin density) when obtained in growth attempts conducted at high temperature, whereas all nanorods are faceted (Figure 1c; low twin density) when grown with furnace temperature. If we assume that (1) there is variation of flux or any other growth parameters along

with the growth time due to unstable growth environment, and (2) the twinning density is strongly dependent on flux or other time-varied growth parameters, then we should also see the transitional structure within these two temperature extremes as well. As we did not observe such phenomenon, we conclude that the variations of flux and growth parameters with time are not the dominant factors in determining the variation of twin density in our system.

Regarding the phase stability, ZnTe crystal is more stable in ZB than in WZ at low temperature.[29] However, high temperature growth was reported to allow nanowires whose stable phase is ZB to access the less stable WZ phase.[25b,28] Consequently, the growth of nanorods at high temperature may contain mixture of segments in WZ, ZB, and other polytypes, in accordance to our SAED and HAADF-STEM observations. The strong relation between twinning and polytypism in the growth of ZnTe is then addressed, since both phenomena are involved simultaneously in the growth at high temperature.

We also relate the twinning density with the diameter of the nanorods. Firstly, as is common in nanostructured materials, there is strong dependence between the as-grown diameter of the structure and the local temperature of the growth.[30] For example, nanowires grown in vapor-liquid-solid (VLS) mechanism are known to have a critical radius of nucleation whose size is inversely proportional to the local temperature.[31] The trend is also reported in ZnO nanowires in a catalyst-free growth from thermal evaporation method,[32] similar to one used in the current work, where the average diameter of ZnO nanowires is increased when the substrate is placed further downstream (away from the center of the furnace where the powder source is located). The correlation between the reduction of diameter and the substrate positioning is associated with the local temperature at the substrate, which affects the deposition and nucleation kinetics and growth thermodynamics. Meanwhile, the influence of other parameters related to the change of positioning away from the source, especially reduction of local vapor pressure, should be less significant. Lower local vapor pressure should result in lower supersaturation level of the nucleus, giving larger nucleus size and nanowire diameter when the substrate is placed away from the source, in contrast to our experimental results.[33] In conclusion, we can safely conclude that the cylindrical rods have smaller diameter due to the high temperature while the faceted rods have a larger diameter since the growth occurred at lower local temperature. The dependence of diameter on temperature also explains the position-dependence morphological transition of hybrid nanorods, with cylindrical segments occurring at the base, which should be at higher temperature than upper segments of the nanorods.

Other researchers also correlated the twining periodicity with the diameter of the nanowire.[25] Studies showed that for III-V type nanowires with diameter above a certain value, the twin-free segments would be wider in larger diameter nanowires. Below such diameter other polytypes may become more stable than the ZB phase, leading to the increase in twinning density and even the formation of WZ segments.[22a,,34] The change in phase stability in small diameter is reasonable since the stability of phases in structures with small surface-to-volume ratio is dominated by the contribution of surface free energies.[35]

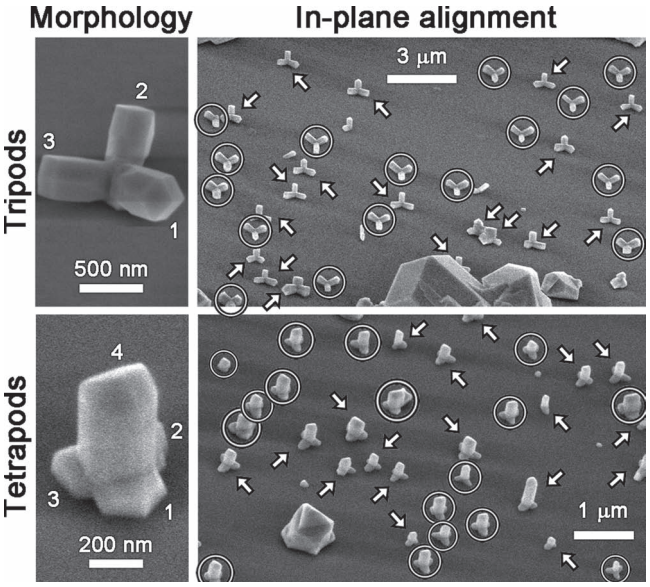


**Figure 3.** SEM images of epitaxial tripods and tetrapods of ZnTe in 45° tilted view. The morphology of the branched nanostructures is clarified, with each of the legs being numbered (tripod: 3 legs, tetrapod: 4 legs). The in-plane alignment of the tripods and tetrapods is exhibited evidently, with the adjacent structures within the same substrate having their legs aligned in only two antiparallel directions. The two possible orientations of tripods and tetrapods are designated with a circle and a white arrow.

Thus, the most stable phase in nanostructures may differ to that in the bulk. Although there have been no calculations performed on the critical diameter of ZnTe for the stable WZ phase, our observation that the twin- and polytypism-rich cylindrical nanorods have small diameters and are grown in higher temperature is in qualitative agreement with previous models on the twinning and polytypism.

## 3. Epitaxial Tripods and Tetrapods: Influence of Polytypism, Twinning, and Polarity on Morphology

### 3.1. Synthesis Products

Beside the growth of nanorods, we were also able to grow branched nanostructures of ZnTe with van der Waals epitaxy in the form of epitaxial nanotripods and nanotetrapods. As shown in **Figure 3**, tripods are crystals with three branches—or "legs"—with three-fold symmetry with respect to the center of the structure. Meanwhile, as the name suggests, tetrapods have four such legs. While the observation of epitaxial tripods has been reported in our previous work, which was more focused on CdS tripods,[6] the structure and phase of ZnTe epitaxial tripods is yet to be established. In addition, the growth of epitaxial tetrapods has never been reported. Thus, this work is the first to document the growth of nanorods, tripods, and tetrapods epitaxially on a single type of substrate, which is accomplished with muscovite mica.

There are two major distinctions in the growth environment to obtain nanorods and branched nanostructures such as

tripods and tetrapods. Tripods and tetrapods were more often observed in muscovite substrates without any surface treatment prior to the growth, in contrast to the growth of nanorods which were typical in substrates with deionized water application (see the Experimental Section). We also consistently observed that tripods and tetrapods are more populated in the downstream region of the substrate which is of lower local temperature, as compared to the nanorods which are more common in the high temperature region of the substrate.

We observed an evident in-plane alignment of the neighboring tripods and tetrapods within the same substrate (Figure 3, also see Supporting Information Figure S4). Adjacent structures are arranged in only two possible orientations. The tripods and tetrapods in these two orientations have been marked differently—with an arrow or a circle—in Figure 3 in order to clarify the presence of the in-plane alignment. The two orientations were actually antiparallel to each other; for a certain leg of a structure, one of the legs from adjacent structures will be either pointing in the same direction or in the opposite direction with the leg concerned. Due to the threefold symmetry of the legs, the two orientations are related by 60° and 180° rotation. Such in-plane alignment has been attributed to the consistency of crystalline relation between the substrate and all structures on the substrate, implying the existence of epitaxy.[6,10] Similar to the case in nanorods, the lattice mismatch between muscovite and ZnTe suggests that van der Waals epitaxy mechanism is also applicable in tripods and tetrapods.

A notable feature of the morphology is the similarity between legs in tripods and tetrapods to that of faceted nanorods (see Figure 1c). Moreover, except for the three additional legs existing close to their base, epitaxial tetrapods closely resemble faceted nanorods since one of the legs are nearly normal to the substrate. The observation of tripods and tetrapods at the low temperature region of the substrate is also consistent with our result in nanorods, for which we concluded that the low local temperature is conducive for the low twinning density necessary to form faceted nanorods.

### 3.2. Characterizations and Growth Mechanism of Epitaxial Tripods

We characterize the structure and crystallinity of tripods to represent the branched epitaxial nanostructures of ZnTe (**Figure 4**). Similar to our previous results on CdS tripods,[6] the polytypic nature of ZnTe tripod is discernible by correlating the observation of HRTEM of a tripod close to its center (Figure 4a) to the resulting SAED pattern of the observed region (Figure 4b). The center of the tripod, which is the junction of all three legs, was of pure ZB phase without any planar defects. However, unlike previous reports of branched crystals from vapor phase,[5a,5b] the legs of ZnTe tripods were also polytypic. As observable within the red- and blue-colored squares in Figure 4a, formation of twin boundaries induces stacking changes and introduces multiple segments of ZB phase to accompany the predominant

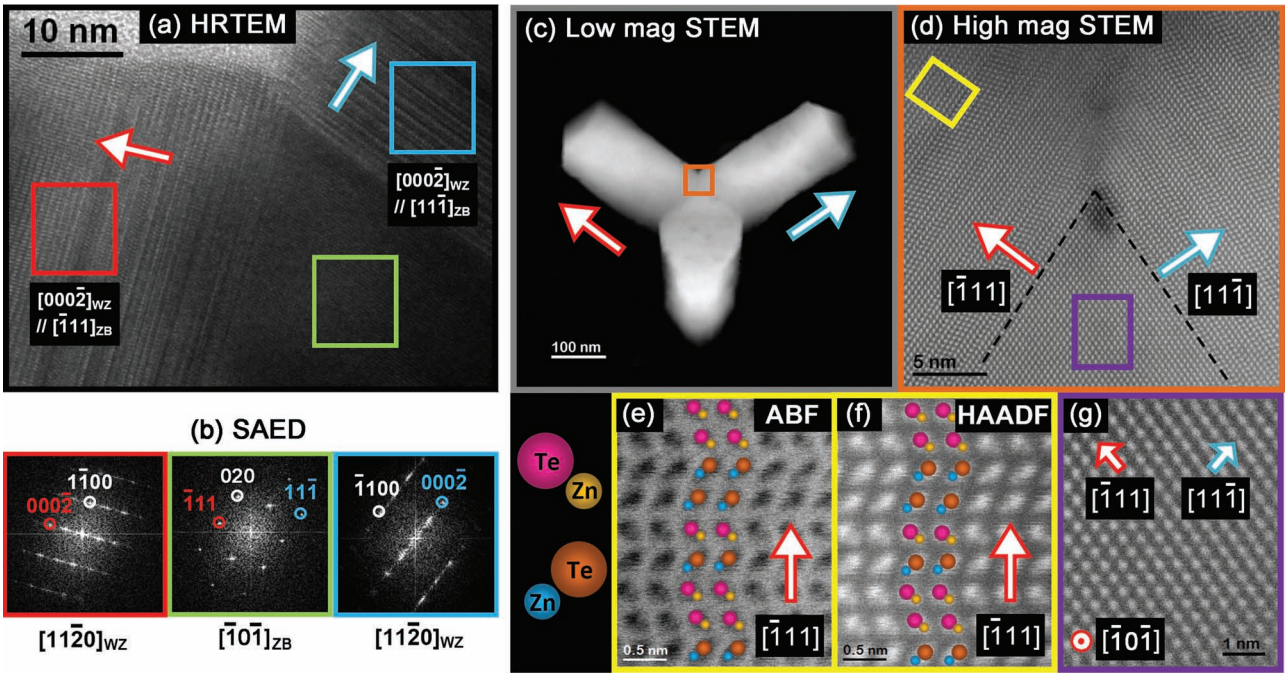


**Figure 4.** Crystallinity characterization of a ZnTe tripod. a) HRTEM image nearby the junction reveals the polytypic nature of the tripod. b) The power spectra from the three regions as marked with colored squares in (a). c) Low magnification STEM image of a complete ZnTe tripod. d) Zoomed-in STEM image of the tripod junction, in the region as indicated with a brown square in (c). The STEM observation is then focused in the region marked with a yellow rectangle by using: e) ABF detector and f) HAADF-detector. We superimposed the columns of atomic dumbbells with spheres in color according to the orientation shown in the illustration to the left of (e). g) The zoomed-in STEM image of region indicated by purple rectangle in (d). In all panels, the white arrow with red (blue) border refers to the growth direction of the left (right) leg, as shown in (c).

existence of WZ phase in the legs. The SAED patterns of the two legs thus feature aligned streaks as the consequence.

HRTEM also reveals that the polytypic legs of the tripod are grown epitaxially from the center. By indexing the power spectrum, the legs of the tripods are found to grow along the *c*-axis, i.e., the ⟨0001⟩ direction. From the alignment of the *c*-axis spots from the FFT pattern of both legs (Figure 4b, left and right) to the ⟨111⟩ spots on the pattern from the center of the tripods which is of pure ZB (Figure 4b, middle), we conclude that the epitaxial relation of the legs on the center of the tripods follows $(\bar{1}11)\langle\bar{1}0\bar{1}\rangle_{ZB} \| (000\bar{1})\langle 11\bar{2}0\rangle_{WZ}$. The structure is consistent with our previous growth model of epitaxial tripods on muscovite via vapor transport method[6] and in accordance with the seeded growth mechanism of tetrapods as proposed by Shiojiri and Kaito.[5a] The growth of branched crystals with the mechanism starts from the nucleation of a seed crystal in pure ZB phase. The seed then assumed an octahedral shape with eight {111}-terminated side facets. As $\{111\}_{ZB}$ is a polar surface, the eight side facets could be divided into two groups: cation-terminated $+\{111\}_{ZB}$ facets (i.e., $111$, $1\bar{1}\bar{1}$, $\bar{1}1\bar{1}$, $\bar{1}\bar{1}1$) and anion-terminated $-\{111\}_{ZB}$ facets (i.e., $\bar{1}\bar{1}\bar{1}$, $\bar{1}11$, $1\bar{1}1$, $11\bar{1}$). Previous reports on branched crystals assumed that further growth on the seed would occur on facets that have the same polarity as the fast growth plane of the particular material. For example, it is assumed in ZnO that only Zn-terminated facets of the octahedra would experience further growth since the O-terminated facets are much less reactive to promote any significant growth.[36] Once the fast growth $\{111\}_{ZB}$ facets of the octahedra are exposed, stacking faults may be introduced to the structure to facilitate a phase transformation to WZ phase for energy minimization. The phase transformation could also occur seamlessly due to the similarity between $\{111\}_{ZB}$ and $\{0001\}_{WZ}$ planes along the stacking direction. As a result, four WZ legs with $\{0001\}_{WZ}$ growth direction would form on the octahedra ZB seed in tetrahedral symmetry, giving rise to tetrapods.[5a] Meanwhile, if the seed is grown epitaxially with one of the fast growth facets to be interfaced with the substrate, only three legs which are upward-inclined from the substrate could be formed, thus resulting in epitaxial tripods.[6]

We aim to confirm the hypothesis of the seeded growth mechanism of branched crystals where the legs of the crystals from a certain compound are assumed to grow in a direction similar to the fast growth plane of other crystal forms of the compounds (i.e., polarity driven growth). To achieve this, we observed the polarity of one of the tripods legs with STEM and confirmed the consistency of the determined growth direction of the legs with that of the nanorods (Figure 2f–j). Figure 4c,d show the location and orientation of the legs which we observed for this purpose. The observation was performed with aberration corrected STEM imaging in annular bright field (ABF, Figure 4e) mode and high angle annular dark field (HAADF, Figure 4f). Both of the complementary STEM modes agreed in showing that the legs of the tripod grew along the Te-direction. Considering the polytypic nature of the legs, we may thus uniquely assign the growth direction of the legs as being the $-\{111\}_{ZB}$ and $-\{0001\}_{WZ}$. Similar to the observation in nanorods, the polarity of the atomic dumbbells of ZnTe is conserved across stacking faults and twinning boundaries that exist within the polytypic leg. Meanwhile, the phase purity of the center of the tripod—necessary for the center to act as a seed—was also verified (Figure 4g).

In conclusion, we confirmed the seeded growth mechanism of tripods. We remark that the existence of pure ZB at the center is reasonable due to the low local temperature growth of tripods. Since the density of twinning is positively correlated with temperature of the growth, the crystals grown at low temperature should have a low density of twinning. Consequently, the low temperature growth allows the formation of a complete octahedral microfaceting to act as the seed to facilitate the subsequent polarity driven growth of tripods or tetrapods. This is in contrast to the case of cylindrical nanorods (Figure 2g,j), as the high density of twins prevents the exposure of the complete octahedral form and results in the growth of nanorods.[37] We also would like to remark that the ZB phase in ZnTe is much more stable than WZ phase, reaching ≈6 meV/atom, which is the largest energy difference among II-VI semiconductors.[29] We believe that the large energy difference is also relevant in explaining why the tripod legs still have some polytypism, whereas previous reports on branched crystals from vapor phase would provide legs that are completely in WZ phase.

## 4. Atomic Modeling of Growth Mechanism

We first note that the syntheses of all structures in this work were performed without any intentional metallic catalyst introduction. Thus, the growth of nanorods is not due to a VLS mechanism. Indeed, there are no remains of pure metallic species specifically located at the tip of nanorods and tripods, as generally observed for VLS growth.[38] Catalyst-free growth of nanostructures in vapor phase is commonly attributed to vapor-solid mechanism. However, we cannot conclusively exclude the possibility of self-catalytic VLS growth since the evaporated ZnTe powder may undergo hydrogen-assisted thermal decomposition into Zn and Te species. In fact, we have shown in our previous work that metallic Te-species could indeed exist at the sidewalls of nanorods,[15] although their mechanism of formation, which could be due to phase segregation, and their role on the growth process are still unclear.

Most of past studies of twinning and polytypism were conducted on catalyzed nanowires. The nucleation of twinning in VLS-grown III-V nanowires is theorized to necessarily be formed on a three phase boundary line between the liquid phase catalyst, the crystallizing nanorods, and the surrounding gaseous environment.[39] Similarly, twinning in a Czochralski grown GaAs bulk crystal is also concluded to occur from a triple phase line between the liquid molten and the crystallized bulk.[27] Hence, the conclusion from previous work implies that a liquid phase during the growth is required to induce twinning during the growth of nanorods, which could only be supplied in our synthesis due to a self-catalyzing agent. Nevertheless, the actual growth mechanism cannot be confirmed in our samples. Moreover, self catalytic VLS is incompatible with the formation of multiple legs in a branched structure, as it is unlikely that each leg was grown with an individual catalyst from the seed.

**Figure 5**a summarizes the growth stages of a ZnTe nanorod, applicable to both cylindrical and faceted nanorods. First, since the growth proceeds on a layer-by-layer basis, we believe that

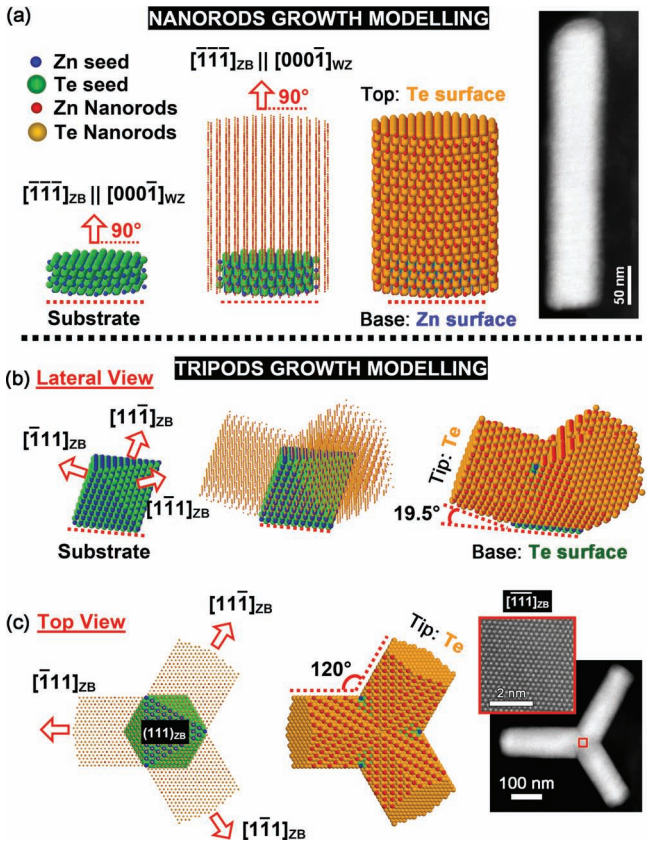


**Figure 5.** The atomic modeling of the growth mechanism of the epitaxial ZnTe nanostructures. a) Growth model of nanorods. A STEM image of the corresponding structure is shown as a comparison. The modeling of the tripods is shown from b) lateral view and c) top view. Animated movies of all atomic models are shown elsewhere.[37]

the growth should start with the nucleation of planar flakes of ZnTe with van der Waals epitaxy. As the nanorods are grown in the Te-terminated direction, the flakes should have their Zn-terminated surface to be interfaced with muscovite. Upon the crystallization, the flakes grow upward in $[\bar{1}\bar{1}\bar{1}]_{ZB}$ direction with octahedra microfaceting containing other {111} sidewall facets as well. However, due to the thermal fluctuation of the environment, stacking misplacement of the next ZnTe bilayers could occur to produce twins or stacking faults. The layer-by-layer growth fashion also ensured that twinning is isolated within a plane, where each atomic bilayer is perfect. The subsequent bilayers of ZnTe can then be written as $[\bar{1}\bar{1}\bar{1}]_{ZB}||[000\bar{1}]_{WZ}$ due to polytypism, with both of the possible phases in Te-directed growth, resulting in a vertically oriented structure.

Figure 5b shows the atomic modeling of growth stages in ZnTe epitaxial tripods. The growth started with the nucleation of a seed with one Te-terminated–{111} facet to be interfaced with the substrate. For low temperature growth, the seed could grow as pure ZB without any twinning, allowing the completion of the seed growth into a {111} octahedra. Meanwhile, since Te-directed growth is the preferred growth direction in ZnTe, only the –{111} facets of the octahedral seed could promote further growth. As one of the –{111} facets is already interfaced with the substrate, the three –{111} facets experienced further growth in the form of upward-inclined legs at an angle of around 19.5° from the substrate.[6] Additionally, the three –{111} facets are symmetrically arranged on the octahedral seed, resulting in 120° separation between adjacent legs when the tripod is viewed from above the substrate (Figure 5c). With an octahedral seed having a triangular facet at the base, the seed could be rotated by 60° or 180° to give a triangular facet with antiparallel direction with respect to the original octahedra. However, both of these orientations have identical atomic arrangements, giving rise to the same epitaxial relationship with the substrate. Correspondingly, two orientations are allowed, resulting into two antiparallel tripod orientations. Therefore, the presence of only two possibilities of in-plane alignment orientation (Figure 3) is also in accordance with the seeded growth mechanism with an octahedra.[6] Animated movies modeling the formation of nanorods and tripods can be found elsewhere.[37]

Regarding the role of the substrate, muscovite mica—by virtue of its layered structure—has been established as a suitable substrate in van der Waals epitaxy of various materials.[10,13] Van der Waals epitaxy mediates the substrate and the atoms at the base of the epitaxial nanostructures with van der Waals interaction, instead of via chemical bonding as in the case of conventional heteroepitaxy.[9] Thus, the usage of muscovite mica allows the alleviation of requirement in lattice matching for the growth of well-crystallized ZnTe nanostructures (≈17% mismatch). Moreover, as van der Waals interactions could arise between induced dipoles, there is no requirement for ionicity to be placed on the surface of muscovite mica. Various crystal planes can be heterointerfaced regardless of the polarity (e.g., $Zn^{2+}$ or $Te^{2-}$ monolayer), as we infer from the STEM data. Furthermore, in the growth of tetrapods (Supporting Information Figure S5 and simulated 3D atomic models[37]), we conclude that it is possible to have other nonpolar planes to be interfaced with the substrate, resulting in the tilted tetrapods via second order twinning seed.[40]

Particular to the result on polarity, we note that muscovite is well-known to have a polar surface with $K^+$ termination.[41] Thus, the conclusion that any polarity of ZnTe could be grown despite the polar surface of mica, combined with the principle in van der Waals epitaxy where chemical bonding and lattice strain is not prominent, means that the substrate has less influence in determining the polarity of nanostructures. This is a major difference between van der Waals epitaxy and conventional homo-/heteroepitaxy, where polar substrates dictate the polarity of overlayer. Not all of the polarity of a material could be interfaced in a conventional epitaxy with a polar substrate since paratwin and inversion of polarity is uncommon. Thus, a specific combination of material and substrate with conventional epitaxy could not produce nanorods (Zn-terminated base) and tripods (Te-terminated base) simultaneously if the material is always growing in only a specific direction, such as along $-[111]_{ZB}$ for ZnTe.

Beside the difference between the polarities of the nucleus formed above the substrate, the growth of nanorods and branched structures differ depending on the way the substrate was prepared prior to growth. Samples with dominant growth of nanorods were obtained with the application of deionized water, whereas the growth of tripods and tetrapods is more common on substrates without such treatment. Differences

between substrates strongly suggest that the application of water to the substrate prior to the growth does have a role in causing the Te-terminated base polarity to be preferable, thus giving rise to vertically oriented structures. However, the exact mechanism responsible for such a phenomenon is still unclear, considering that water molecules possibly adsorbing onto the substrate are supposed to be evaporated during the high temperature growth.

## 5. Conclusions

We have reported the growth of epitaxial nanorods, tripods, and tetrapods of ZnTe on muscovite mica substrate. We present a fundamental insight as we demonstrate that the selection of morphology of nanostructures from van der Waals epitaxy has an underlying basis: that crystallinity and polarity play important roles in selecting the manifested macro-morphology of nanostructures. Based on intensive structural and crystallinity characterization with electron microscopy, we conclude that twinning, polytypism, and polarity were the decisive phenomena in facilitating the morphological transition between cylindrical and faceted nanorods, and the formation of branched nanostructures in the form of tripods and tetrapods. We also constructed the growth models for the three epitaxial structures. Particularly, we consider that the primary distinction for the growth of the three structures started from the initial formation of nucleus: (i) flat flake-like seed with a Zn-terminated base for nanorods, (ii) octahedral seed with Te-terminated base for tripods, and (iii) second-order twinned octahedral structures seed with a truncated octahedra as the first seed for tetrapods. We believe that the possibility to contain various seed polarities is a feature of growth in van der Waals epitaxy, for the first time resulting in variation of epitaxial structures within only a single type of substrate.

Our results served as a potential scheme in modulating the morphology of nanostructures in van der Waals epitaxy by exploiting the effects of twinning, polytypism, and polarity. With such scheme, we believe that it is possible to produce even more complex architectures, subject to the controllability of environment during the growth process. The richness of aspects in nanostructural growth—many of which yet to be investigated in van der Waals epitaxy—also showed that there are ample research opportunities in the van der Waals epitaxy of nanostructures.

## 6. Experimental Section

All samples were synthesized using a home-built vapor transport system. A sheet of (001) muscovite mica ($KAl_2(Si_3Al)O_{10}(OH)_2$, muscovite-$2M_1$, research grade)[10] was cut into pieces and air-cleaved, to be used as the substrate with the freshly cleaved surface facing upward. For the growth of nanorods, deionized water was drop-cast onto the substrate and left for 5 min before the substrate was blow-dried. Meanwhile, no surface treatment on the substrate was conducted for the growth of tripods and tetrapods. The substrate was positioned downstream inside a quartz tube mounted on a single zone furnace (Lindberg/Blue M TF55035C-1), with its upstream edge at a distance of 13 cm from the center of the furnace. ZnTe powder (99.99%, Alfa Aesar) was put into a quartz boat, which was located in the center of the furnace. The vapor transport system was evacuated to the base pressure of ≈20 mTorr, after which 30 sccm of Ar gas premixed with 5% $H_2$ was flown to allow the system to stabilize at 50 Torr. The temperature of the furnace was thus elevated to 750–850 °C, kept constant for 30 min, and allowed to reach room temperature naturally.

Morphology and crystallinity characterizations were performed with field-emission SEM (JEOL JSM-7001F) and HRTEM (JEOL 2010F with a field emission gun operated at 200 kV). Aberration-corrected HAADF-STEM and ABF-STEM were performed on a FEI Titan 60–300 keV operated at 300 kV. The as-grown samples were dispersed in isopropanol by ultrasonication, followed by the drop-casting of the suspension to a lacey carbon grid (Electron Microscopy Sciences) for ABF-STEM and HAADF-STEM observation. Geometric 3D atomic models of the growth mechanism were constructed using the Rhodius software.[42]

## Acknowledgements

M.I.B.U. and M.d.l.M. contributed equally to this work. Q.X. acknowledges the strong support from the Singapore National Research Foundation through a fellowship grant (NRF-RF2009-06), and from Nanyang Technological University through a generous start-up grant (M58110061) and the New Initiative Fund (M58110100). J.A. acknowledges funding from the Spanish MICINN projects MAT2010-15138 (COPEON) and CSD2009-00013 (IMAGINE) and Generalitat de Catalunya (2009 SGR 770 and NanoAraCat). The authors thank the staff at the TEM facilities at INA-LMA.

Received: July 18, 2012
Revised: September 12, 2012
Published online: October 29, 2012

[1] M. I. B. Utama, J. Zhang, R. Chen, X. Xu, D. Li, H. Sun, Q. H. Xiong, *Nanoscale* **2012**, *4*, 1422.
[2] a) S. Mardix, *Phys. Rev. B* **1986**, *33*, 8677; b) E. Alexander, Z. H. Kalman, S. Mardix, I. T. Steinberger, *Philos. Mag.* **1970**, *21*, 1237.
[3] Y. Ding, Z. L. Wang, *J. Phys. Chem. B* **2004**, *108*, 12280.
[4] J. Bao, D. C. Bell, F. Capasso, J. B. Wagner, T. Mårtensson, J. Trägårdh, L. Samuelson, *Nano Lett.* **2008**, *8*, 836.
[5] a) M. Shiojiri, C. Kaito, *J. Cryst. Growth* **1981**, *52*, 173; b) H. Iwanaga, M. Fujii, S. Takeuchi, *J. Cryst. Growth* **1993**, *134*, 275; c) L. Manna, E. C. Scher, A. P. Alivisatos, *J. Am. Chem. Soc.* **2000**, *122*, 12700.
[6] M. I. B. Utama, Q. Zhang, S. F. Jia, D. H. Li, J. B. Wang, Q. H. Xiong, *ACS Nano* **2012**, *6*, 2281.
[7] M. de la Mata, C. Magen, J. Gazquez, M. I. B. Utama, M. Heiss, S. Lopatin, F. Furtmayr, C. J. Fernández-Rojas, B. Peng, J. R. Morante, R. Rurali, M. Eickhoff, A. Fontcuberta i Morral, Q. Xiong, J. Arbiol, *Nano Lett.* **2012**, *12*, 2579.
[8] J. E. Ayers, *Heteroepitaxy of Semiconductors: Theory, Growth, and Characterization*, CRC Press, Boca Raton, FL **2007**.
[9] A. Koma, K. Sunouchi, T. Miyajima, *Microelectron. Eng.* **1984**, *2*, 129.
[10] M. I. B. Utama, F. J. Belarre, C. Magen, B. Peng, J. Arbiol, Q. H. Xiong, *Nano Lett.* **2012**, *12*, 2146.
[11] a) M. I. B. Utama, Z. P. Peng, R. Chen, B. Peng, X. L. Xu, Y. J. Dong, L. M. Wong, S. J. Wang, H. D. Sun, Q. H. Xiong, *Nano Lett.* **2011**, *11*, 3051; b) J. Pan, M. I. B. Utama, Q. Zhang, X. F. Liu, B. Peng, L. M. Wong, T. C. Sum, S. J. Wang, Q. H. Xiong, *Adv. Mater.* **2012**, *24*, 4151; c) R. Chen, M. I. B. Utama, Z. Peng, B. Peng, Q. H. Xiong, H. Sun, *Adv. Mater.* **2011**, *23*, 1404; d) Y. J. Hong, T. Fukui, *ACS Nano* **2011**, *5*, 7576; e) H. Peng, W. Dang, J. Cao, Y. Chen, D. Wu, W. Zheng, H. Li, Z.-X. Shen, Z. Liu, *Nat. Chem.* **2012**, *4*, 281.
[12] Y. K. A. Lau, D. J. Chernak, M. J. Bierman, S. Jin, *J. Mater. Chem.* **2009**, *19*, 934.

[13] a) K. Ueno, K. Saiki, T. Shimada, A. Koma, *J. Vac. Sci. Technol., A* **1990**, *8*, 68; b) K. Saiki, K. Ueno, T. Shimada, A. Koma, *J. Cryst. Growth* **1989**, *95*, 603.
[14] J. Zhang, P.-C. Chen, G. Shen, J. He, A. Kumbhar, C. Zhou, J. Fang, *Angew. Chem. Int. Ed.* **2008**, *47*, 9469.
[15] Q. Zhang, J. Zhang, M. I. B. Utama, B. Peng, M. de la Mata, J. Arbiol, Q. H. Xiong, *Phys. Rev. B* **2012**, *85*, 085418.
[16] a) Y. L. Cao, Z. T. Liu, L. M. Chen, Y. B. Tang, L. B. Luo, J. S. Jie, W. J. Zhang, S. T. Lee, C. S. Lee, *Opt. Express* **2011**, *19*, 6100; b) Z. Li, J. Salfi, C. De Souza, P. Sun, S. V. Nair, H. E. Ruda, *Appl. Phys. Lett.* **2010**, *97*, 063510.
[17] N. Mingo, *Appl. Phys. Lett.* **2004**, *85*, 5986.
[18] a) S. Li, Y. Jiang, D. Wu, B. Wang, Y. Zhang, J. Li, X. Liu, H. Zhong, L. Chen, J. Jie, *Appl. Phys. A: Mater. Sci. Process.* **2011**, *102*, 469; b) K.-T. Yong, Y. Sahoo, H. Zeng, M. T. Swihart, J. R. Minter, P. N. Prasad, *Chem. Mater.* **2007**, *19*, 4108; c) D. D. Fanfair, B. A. Korgel, *Cryst. Growth Des.* **2008**, *8*, 3246; d) E. Janik, P. Dłużewski, S. Kret, A. Presz, H. Kirmse, W. Neumann, W. Zaleszczyk, L. T. Baczewski, A. Petroutchik, E. Dynowska, J. Sadowski, W. Caliebe, G. Karczewski, T. Wojtowicz, *Nanotechnology* **2007**, *18*, 475606.
[19] E. Janik, J. Sadowski, P. Dluzewski, S. Kret, L. T. Baczewski, A. Petroutchik, E. Lusakowska, J. Wrobel, W. Zaleszczyk, G. Karczewski, T. Wojtowicz, A. Presz, *Appl. Phys. Lett.* **2006**, *89*, 133114.
[20] D. Spirkoska, J. Arbiol, A. Gustafsson, S. Conesa-Boj, F. Glas, I. Zardo, M. Heigoldt, M. H. Gass, A. L. Bleloch, S. Estrade, M. Kaniber, J. Rossler, F. Peiro, J. R. Morante, G. Abstreiter, L. Samuelson, A. Fontcuberta i Morral, *Phys. Rev. B* **2009**, *80*, 245325.
[21] J. Arbiol, A. Fontcuberta i Morral, S. Estrade, F. Peiro, B. Kalache, P. Roca i Cabarrocas, J. R. Morante, *J. Appl. Phys.* **2008**, *104*, 064312.
[22] a) V. G. Dubrovskii, N. V. Sibirev, *Phys. Rev. B* **2008**, *77*, 035414; b) Y. Hao, G. Meng, Z. L. Wang, C. Ye, L. Zhang, *Nano Lett.* **2006**, *6*, 1650.
[23] a) M. J. Bierman, Y. K. A. Lau, A. V. Kvit, A. L. Schmitt, S. Jin, *Science* **2008**, *320*, 1060; b) S. A. Morin, S. Jin, *Nano Lett.* **2010**, *10*, 3459.
[24] J. Johansson, L. S. Karlsson, C. Patrik T. Svensson, T. Martensson, B. A. Wacaser, K. Deppert, L. Samuelson, W. Seifert, *Nat. Mater.* **2006**, *5*, 574.
[25] a) R. E. Algra, M. A. Verheijen, M. T. Borgstrom, L.-F. Feiner, G. Immink, W. J. P. van Enckevort, E. Vlieg, E. P. A. M. Bakkers, *Nature* **2008**, *456*, 369; b) P. Caroff, K. A. Dick, J. Johansson, M. E. Messing, K. Deppert, L. Samuelson, *Nat. Nanotechnol.* **2009**, *4*, 50.
[26] F. M. Davidson, D. C. Lee, D. D. Fanfair, B. A. Korgel, *J. Phys. Chem. C* **2007**, *111*, 2929.
[27] D. T. J. Hurle, *J. Cryst. Growth* **1995**, *147*, 239.
[28] a) M. Koguchi, H. Kakibayashi, M. Yazawa, K. Hiruma, T. Katsuyama, *Jpn. J. Appl. Phys.* **1991**, *31*, 2061; b) K. A. Dick, P. Caroff, J. Bolinsson, M. E. Messing, J. Johansson, K. Deppert, L. R. Wallenberg, L. Samuelson, *Semicond. Sci. Technol.* **2010**, *25*, 024009.
[29] C. Y. Yeh, Z. W. Lu, S. Froyen, A. Zunger, *Phys. Rev. B* **1992**, *46*, 10086.
[30] S. Bandow, S. Asaka, Y. Saito, A. M. Rao, L. Grigorian, E. Richter, P. C. Eklund, *Phys. Rev. Lett.* **1998**, *80*, 3779.
[31] R. S. Wagner, W. C. Ellis, *Trans. Metall. Soc. AIME* **1965**, *223*, 1053.
[32] J. Li, Q. Zhang, H. Peng, H. O. Everitt, L. Qin, J. Liu, *J. Phys. Chem. C* **2009**, *113*, 3950.
[33] a) Y. X. Zhang, Y. Tang, K. Lee, M. Ouyang, *Nano Lett.* **2009**, *9*, 437; b) L. Su, Z. Xiaozhong, Y. Bin, Y. Ting, *Nanotechnology* **2009**, *20*, 495604.
[34] T. Akiyama, K. Sano, K. Nakamura, T. Ito, *Jpn. J. Appl. Phys.* **2006**, *45*, L275.
[35] R. Leitsmann, F. Bechstedt, *J. Appl. Phys.* **2007**, *102*, 063528.
[36] Y. Ding, Z. L. Wang, T. J. Sun, J. S. Qiu, *Appl. Phys. Lett.* **2007**, *90*, 153510.
[37] Animated 3D atomic models showing the polarity-driven growth mechanism of nanorod, tripod and tetrapod can be found on the web: http://www.icmab.es/gaen/research/179 (last accessed October 2012).
[38] R. S. Wagner, W. C. Ellis, *Appl. Phys. Lett.* **1964**, *4*, 89.
[39] F. Glas, J.-C. Harmand, G. Patriarche, *Phys. Rev. Lett.* **2007**, *99*, 146101.
[40] E. Uccelli, J. Arbiol, C. Magen, P. Krogstrup, E. Russo-Averchi, M. Heiss, G. Mugny, F. Morier-Genoud, J. Nygård, J. R. Morante, A. Fontcuberta i Morral, *Nano Lett.* **2011**, *11*, 3827.
[41] K. Müller, C. C. Chang, *Surf. Sci.* **1969**, *14*, 39.
[42] S. Bernal, F. J. Botana, J. J. Calvino, C. López-Cartes, J. A. Pérez-Omil, J. M. Rodríguez-Izquierdo, *Ultramicroscopy* **1998**, *72*, 135.